SAND2016-11740R

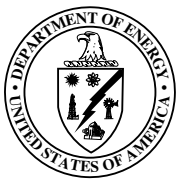

Sandia National Laboratories

Operated for the U.S. Department of Energy by

Sandia Corporation

Albuquerque, New Mexico 87185

date: September 22, 2016

to: Benjamin Reedlunn

from: Edmundo Corona, Org. 1554, MS-0840

subject: Shear-dominated failure in the 'hat' specimen from the 2013 Sandia Fracture Challenge.

Introduction

The objective of this memo is to present a brief report of the progress achieved during FY2016 on the investigation of ductile failure in the 2013 Sandia Fracture Challenge specimen. It is a follow-up to the results of an experimental investigation presented in [1]. The experimental investigation was conducted with both the original steel A286 material used in the fracture challenge as well as with Al 7075-T651. The new results include further microscopy work for the steel A286 specimens, failure criterion verification for both materials and the implementation of a finite element model containing 'material imperfections' to simulate the limit load in the response of the steel A286 specimens. Funding used to conduct the work presented here was provided by the ASC V&V program on validation of shear failure (Benjamin Reedlunn, PI) and from Sandia's LDRD program. This memo assumes that the reader is familiar with the material in [1].

Further Microscopy Work for Steel A286 Specimens

The photographs in Figs. 23 and 24 in [1] showed many point-like features similar to the ones shown in the top right photograph in Fig. 1. The higher magnification images shown here demonstrate that these features are second-phase inclusions in the material. Further SEM analysis indicated that these second-phase inclusions were titanium carbide.

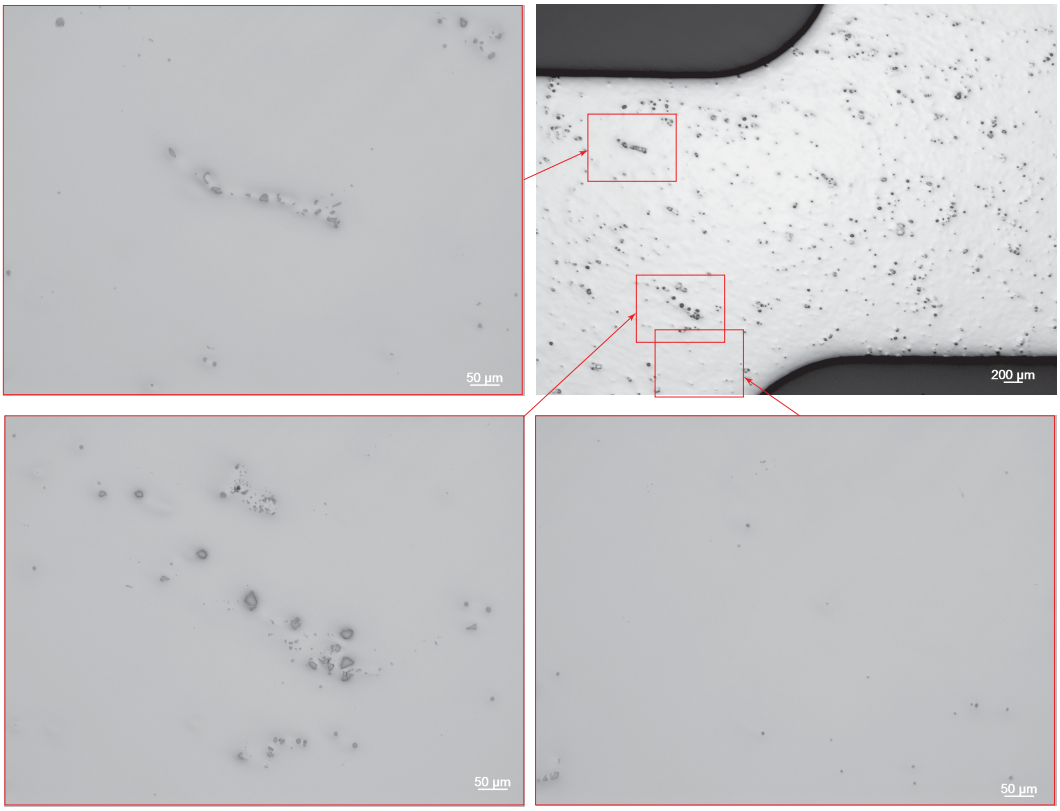

Figure 1. Polished surface of an untested specimen at two magnifications showing that the point-like feature in the lower magnification image are second phase inclusions.

The steel A286 specimens displayed load-deflection curves that achieved a maximum followed by a gradual reduction in load to the point of failure, as shown in Fig. 15 in [1]. Although the above mentioned photographs in [1] clearly showed fracture propagation through the two regions with high shear was responsible for the decrease in load, they did not clearly show how failure initiated. New photographs taken at higher magnification gave a better idea. Figure 2 shows the progression seen from specimens S2, S3, S4 at the center plane of the specimen. Figure 2(b) shows that the blunt notches seen for specimen S3 in are regions of material failure that display several fracture surfaces, giving the appearance of a blunt feature when looking with lower magnification. Looking at specimen S4 in Fig. 2(c) shows that although several cracks started form the horizontal surface, it seems that the one closest to the left prevailed as the main crack, thus forming what were called 'indentations' in [1]. The hypothesis is that the first cracks that formed were a little to the right of the final main crack but stopped growing when cracks to the left developed and penetrated deeper into the specimen.

Figure 3 shows the same progression but on the surface plane of the specimen. Note that specimen S3 in Fig. 3 shows evidence of small cracks, perhaps in a less torturous fashion, and that specimen S4 shows a much cleaner surface on the right surface. As indicated in [1], long, thinner cracks eventually develop from the indentations on the surface of the specimen.

Figures 4 and 5 show images of the four fillets of specimen S3 at the center and surface planes, respectively, showing the damage was, for the most part, similar in all corners, but different between the center and surface planes. Clearly the curvature of the horizontal surfaces is more visible in Fig. 5, while the amount of damage is more pronounced in Fig. 4. This suggests that the point of first failure is at the roots of the fillets in the center plane of the specimen.

Finally, Fig. 6 shows photographs at different magnifications of the vicinity of the failure surface of a notched tension specimen with $r/R = 0.32$. The cut shown is diametrical. The figure shows that inclusions near the surface broke and formed cavities. Broken inclusions were also prevalent in the hat specimens, as can be seen in Figs. 27 through 29 in [1]. Under shear, however, the broken inclusions gave rise to very elongated, crack-like cavities, unlike the much less severely elongated ones in the notched specimen. This is an indication of the much higher material deformation achieved in the shear dominated hat specimens. Still, the breaking of the second-phase inclusions seems to be an important aspect of the failure of the material. The matrix material, however, seems to have great ductility, especially under shear.

One final aspect that was investigated via microscopy was the fuzzy nature of the shear specimen surface seen in all the photographs presented here. The principal question to answer is whether the surface was rough from the start or it roughened during deformation. Photographs taken at locations far from areas of high stress, where the material remained elastic such as in Fig. 7 (a) indicate that the surface roughness was a result of the wire EDM process used to manufacture the specimen. Whether this surface roughness has an effect on when failure occurs in the specimen remains unknown, although clearly cracks can form

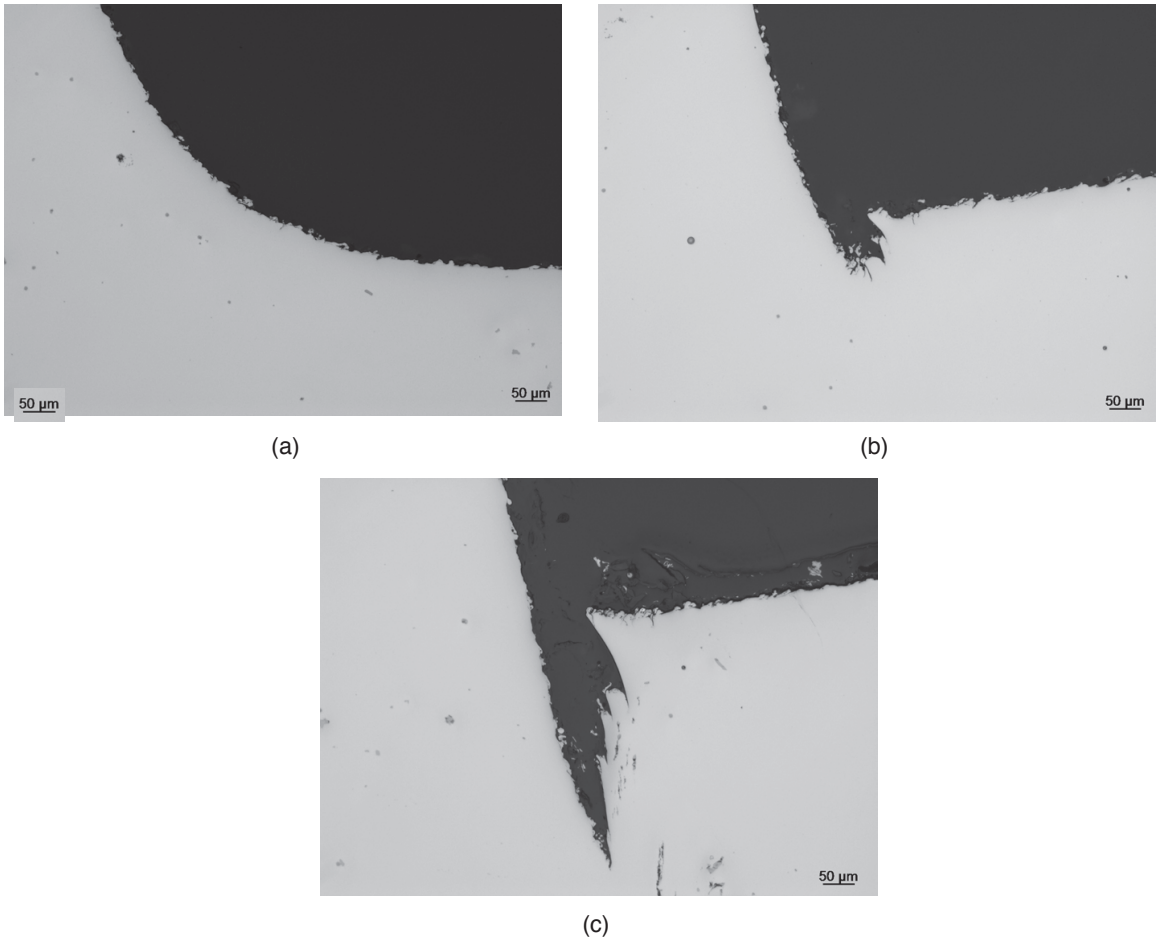

Figure 2. Examples of progression of damage in the area where material damage was first observed at the center plane of the specimens. (a) Specimen S2, (b) specimen S3 and (c) specimen S4.

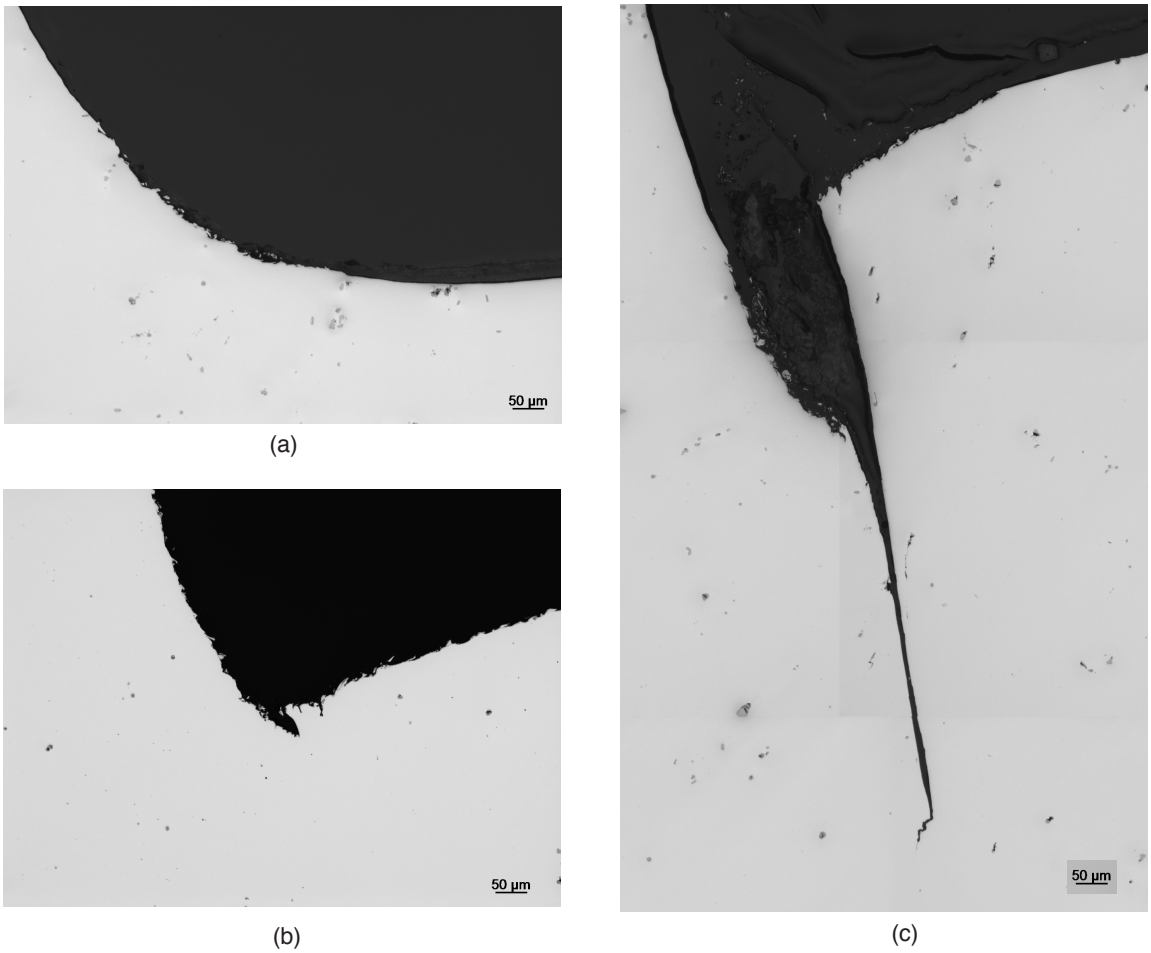

Figure 3. Examples of progression of damage on the surface plane of the specimens. (a) Specimen S2, (b) specimen S3 and (d) specimen S4.

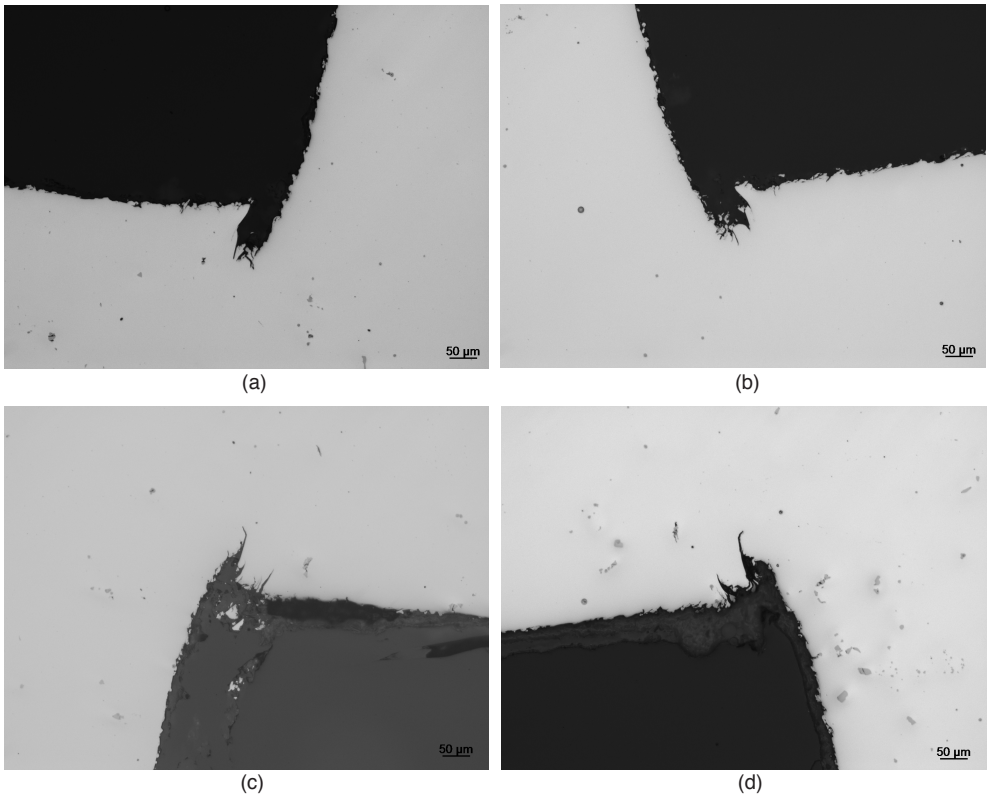

Figure 4. Comparison of the state at the four fillets where damage was first detected at the center of specimen S3.

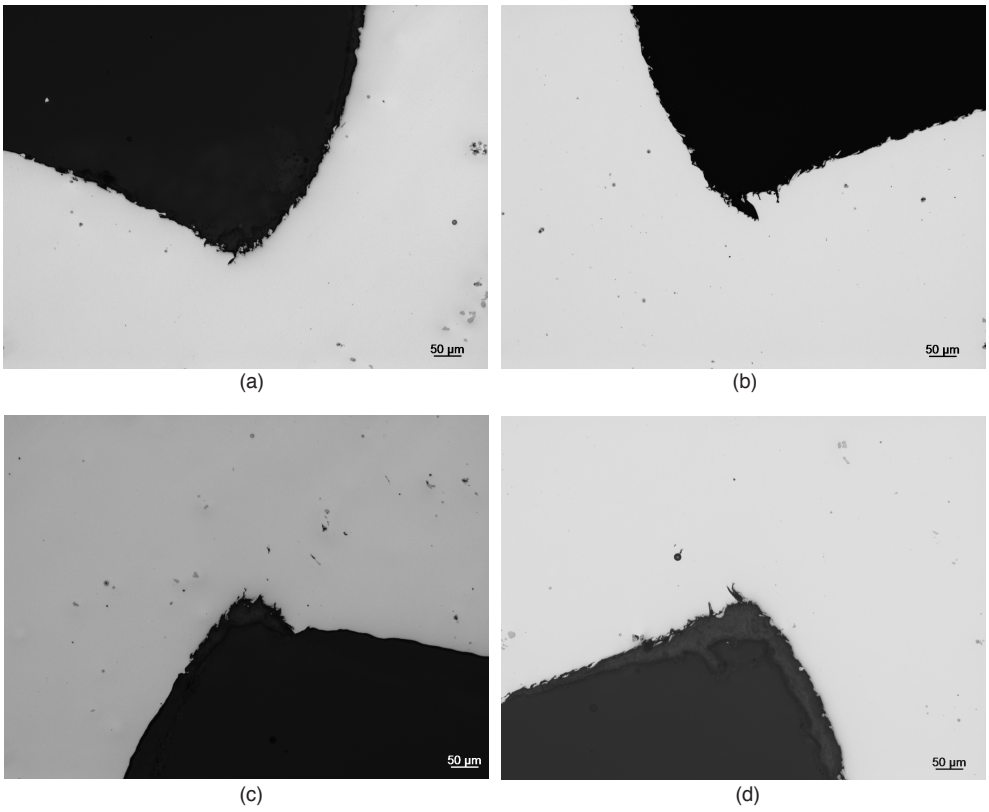

Figure 5. Comparison of the state at the four fillets at the surface of specimen S3.

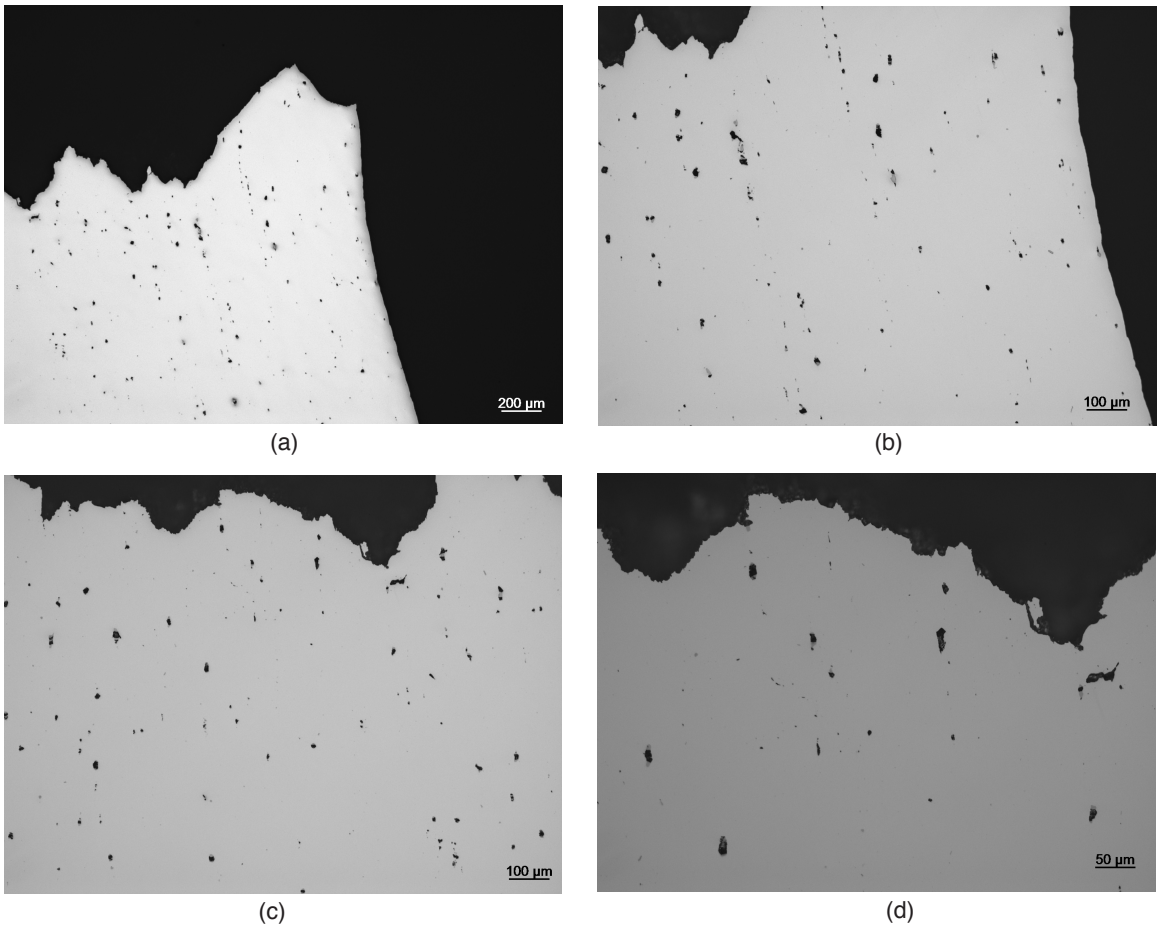

Figure 6. Post-failure micrographs of a diametrically cut notched tensile specimen with $r/R = 3.2$. (a) Near the edge, (b) near the edge with higher magnification, (c) near the center and (d) near the center with higher magnification.

from the surface as shown in Fig. 7(b) for a region just to the right of the fillet in Fig. 2(b).

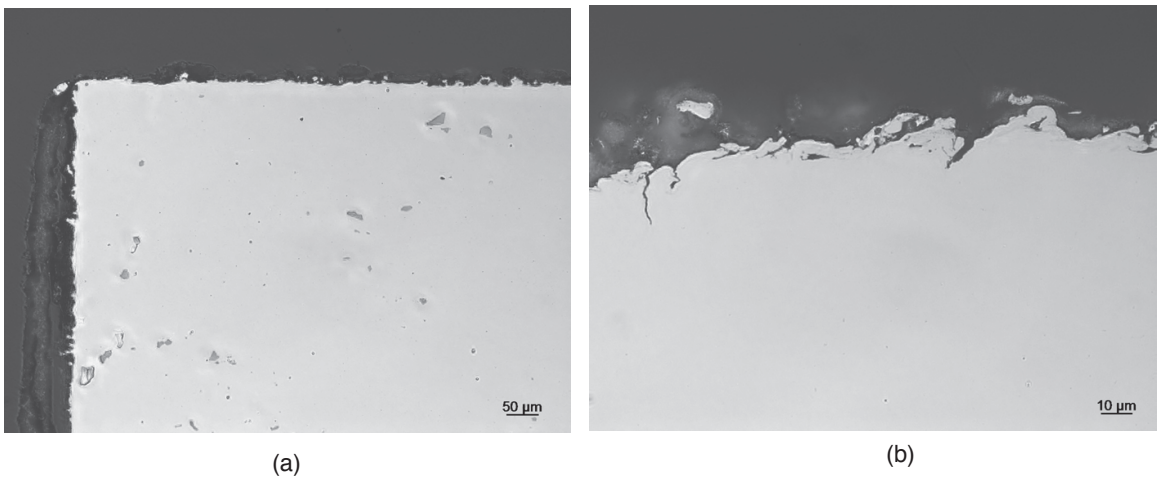

Figure 7. (a) Surface roughness in region that remained essentially unloaded in the test and (b) high-magnification image showing cracks extending from the surface just to the right of the fillet shown in Fig. 2(b).

Failure Criterion Investigation

Al 7075

In order to investigate the ability of the Johnson-Cook failure model [2] to fit the data obtained, a finite element model of the specimen was first constructed within the Abaqus/Explicit program. The geometric model is shown in Fig. 8. It takes advantage of two planes of symmetry in the specimen. The elements are eight node hexahedrals with reduced integration and hourgalss control. Element size studies indicated that elements of size 0.005 inches on the side gave reasonably well converged results. For reference, the heigh of the segment undergoing shear is 0.125 inches. The speed of loading was in the order of 0.04 inches in 0.01 seconds using the smooth step option. Varying the speed of loading a decade above this value confirmed no rate sensitivity in the solution. The constitutive model was J_2 isotropic hardening plasticity with a power-law hardening fit for the stress-strain curve. The parameters of the stress-strain curve and of the failure criterion were determined in [3].

Figure 9 shows comparisons between the measured and predicted load-deflection curves. The labels High, Mid, and Low refer to the three fits for the failure criterion proposed in [3]. The constitutive model is the same in the three cases; therefore, they differ only on the failure point indicated by $\times$. The calculated responses overestimate the load because the material is actually anisotropic. Accounting for the anisotropy in the simplest possible way through the Hill yield criterion gives reasonable agreement of the load-deflection responses. Yet, the failure model was only exercised with the J_2 model.

Figure 10 (a) shows contours of the Johnson-Cook damage parameter on the surface plane of the model, where it reaches its maximum value just before the failure point for the Mid

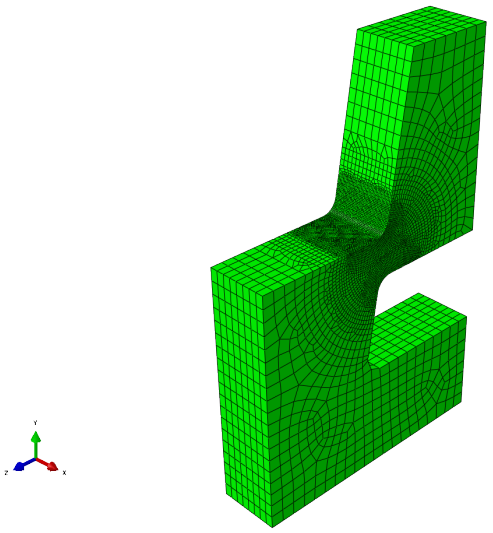

Figure 8. Finite element model.

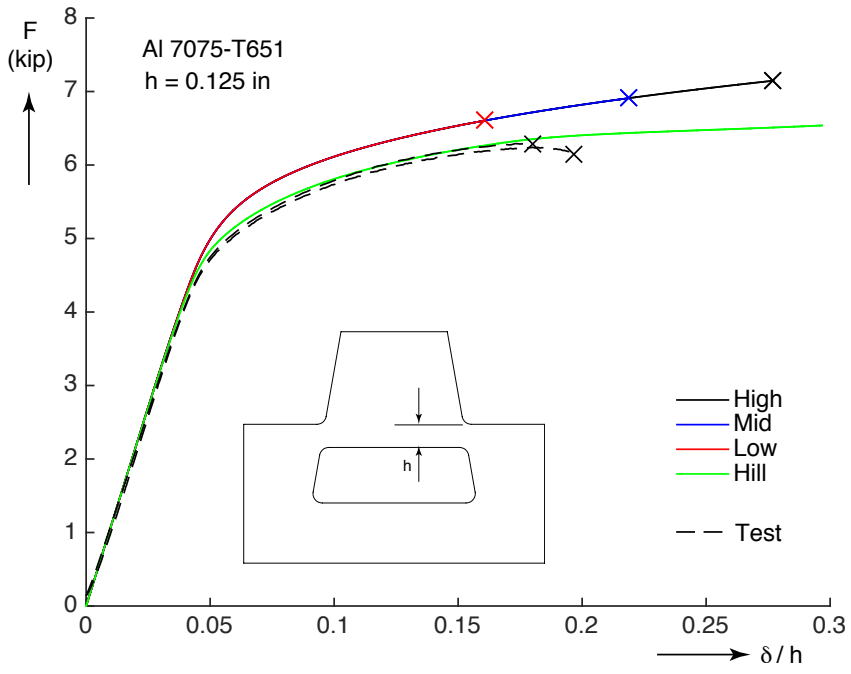

Figure 9. Comparison of the predicted and measured load-deflection responses of the Al 7075 hat specimens.

failure properties. Deep red indicates high damage. Figure 10(b) shows the stress triaxiality on the same surface. Clearly the maximum damage occurs whithin a shear-dominated region of nearly zero triaxiality. For comparison, Figs. 11(a) and (b) show similar contours on the center surface showing smaller damage and mostly negative triaxiality in the high damage region.

The plot of equivalent plastic strain vs. triaxiality used for calibration of the model in [3] is shown in Fig. 12. The circular symbols indicate the combinations in the most critical element in the notched and smooth tension test specimen models at the same displacements as when failure occurred in the tests. The plot for the hat specimen has now been added to the figure. It shows that the triaxiality was just slightly negative for most of the time, and that, by matching the displacement at failure with the test data the equivalent plastic strain and triaxiality combination at the most critical element fell within the Johnson-Cook curves calibrated from the tensile-dominated data. The Med curve is the most preferred one. Note, however, that since no other test data are available at low triaxialities, nothing can be said about the potential spread of the data.

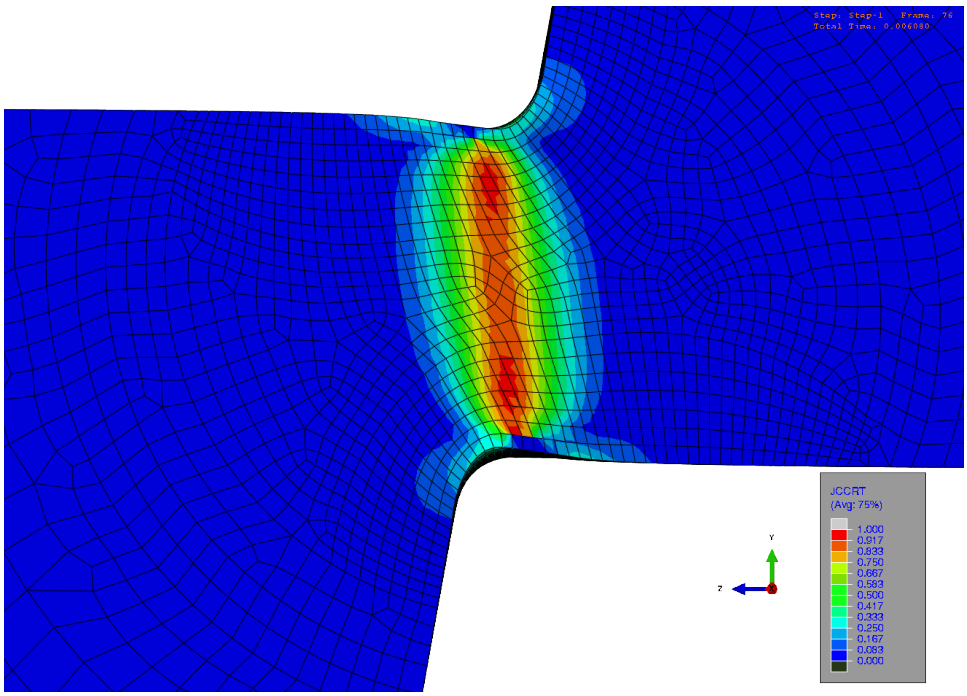

(a)

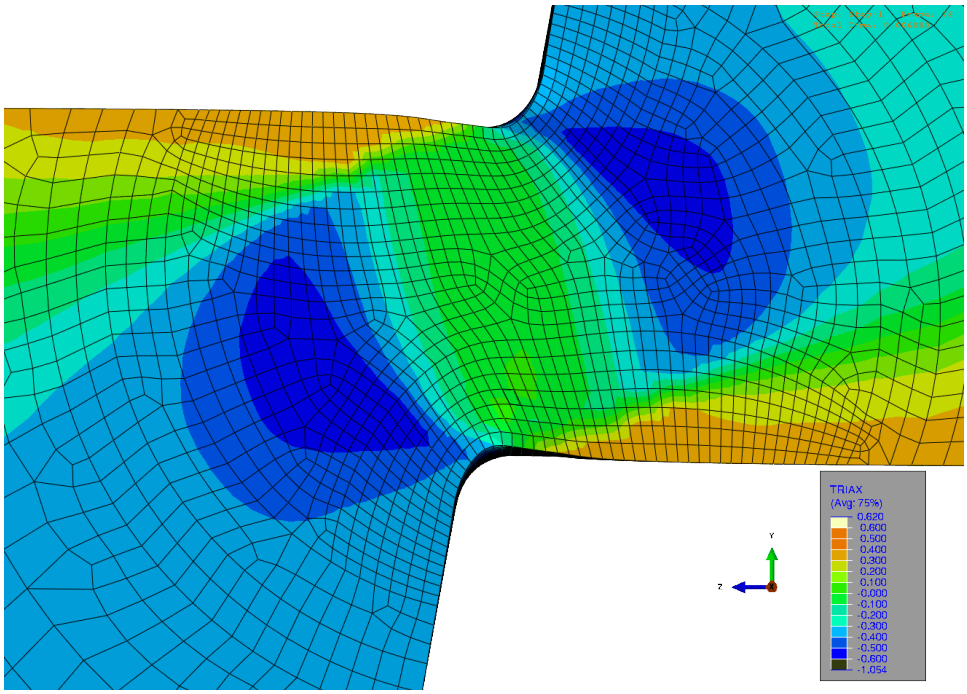

(b)

Figure 10. Damage state at the surface of the specimen. (a) Johnson-Cook damage and (b) triaxiality.

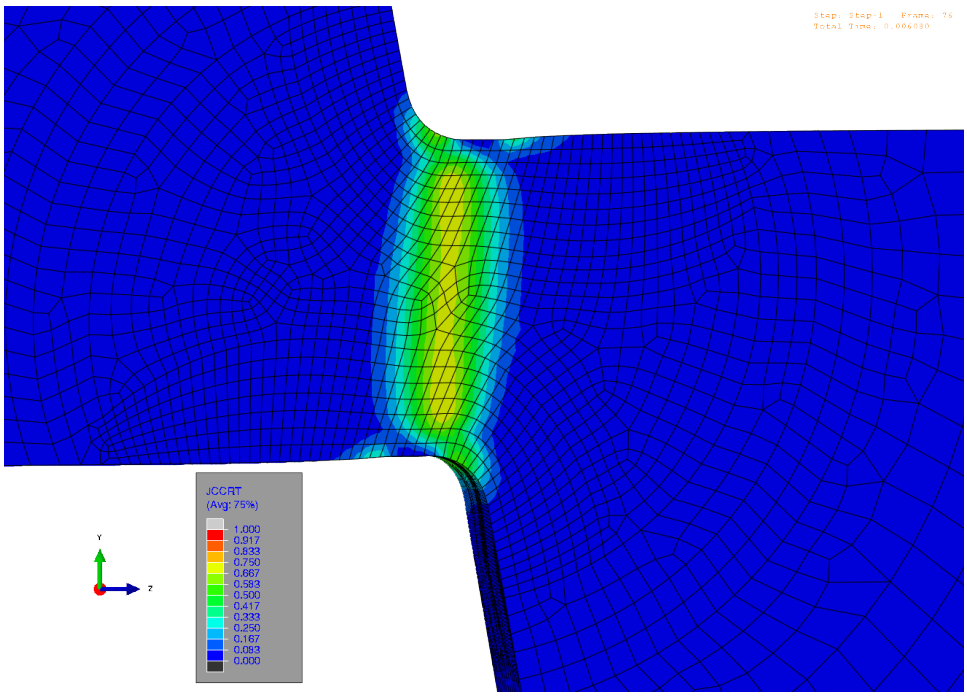

(a)

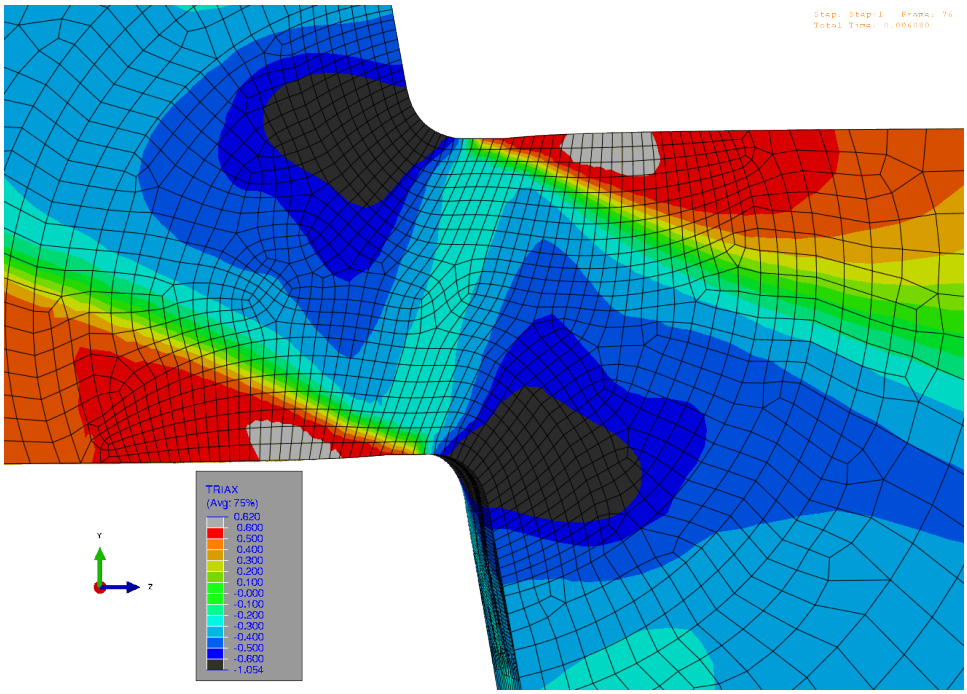

(b)

Figure 11. Damage state at the center plane of the specimen. (a) Johnson-Cook damage and (b) triaxiality.

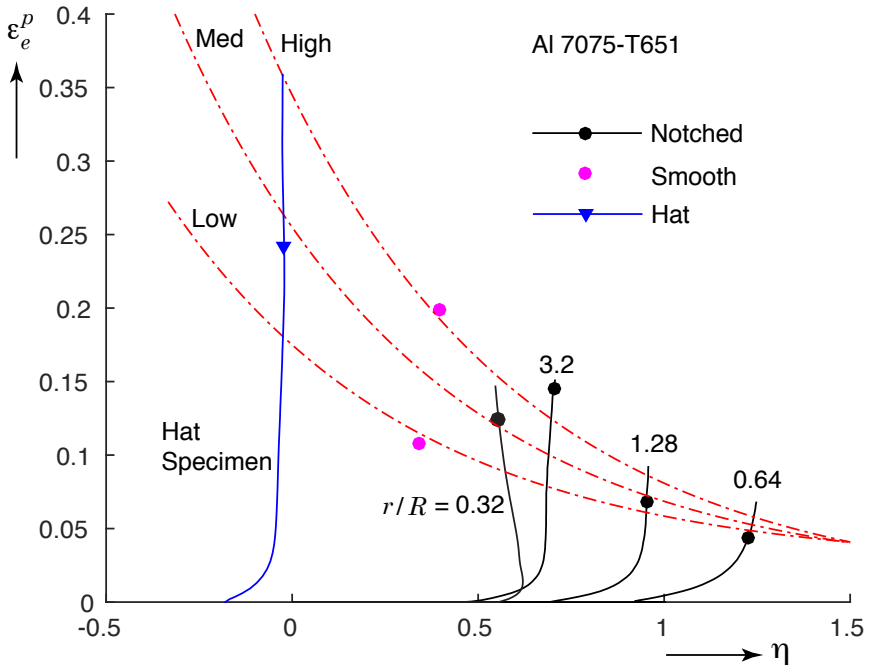

Figure 12. Plot of equivalent plastic strain vs. triaxiality at the models' critical elements, including results from notched tension, smooth tension and hat specimens.

Steel A286

For this material, the simulation of the test was conducted using similar model geometry and loading procedures as before. Because of the higher ductility of this material the speed of loading was 0.07 inches in 0.01 seconds and the element size was 0.002 inches. Also, the equivalent stress-strain curve was fitted using a piecewise linear fit, and a Hill model to account for the yield anisotropy was used. Figure 13 shows the comparison between the simulation and test results for the load-deflection response. Clearly the simulation does not develop the maximum load observed in the tests. In fact, the failure criterion, whose calibration is shown in Fig. 14 was never satisfied. It is then not surprising that the limit load was not predicted since it was shown previously that it is induced by failure of the material.

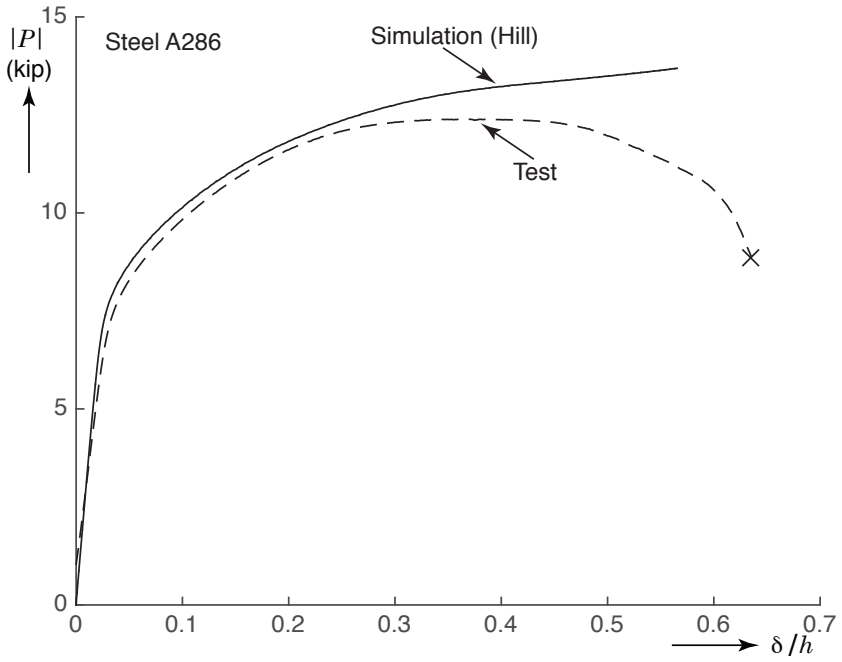

Figure 13. Comparison of the predicted and measured load-deflection responses of the steel A286 hat specimen.

Figures 15(a) and (b) shows the damage in both surface and center planes at the end of the simulation. They show about the same amount of damage at the critical locations on both sides. Note that small indentations are seen in the center plane at the top and bottom of the high damage zone, but unlike in the tests, these are due strictly to material deformation. The equivalent plastic strain vs. triaxiality plots at the most critical elements in the surface and center planes are shown in Fig. 16(a). The points marked S3 show when the specimen reached the same displacement as the unloading point of specimen S3. The plot in Fig. 16(b) shows the damage at the same two points plotted vs. the deflection of the specimen.

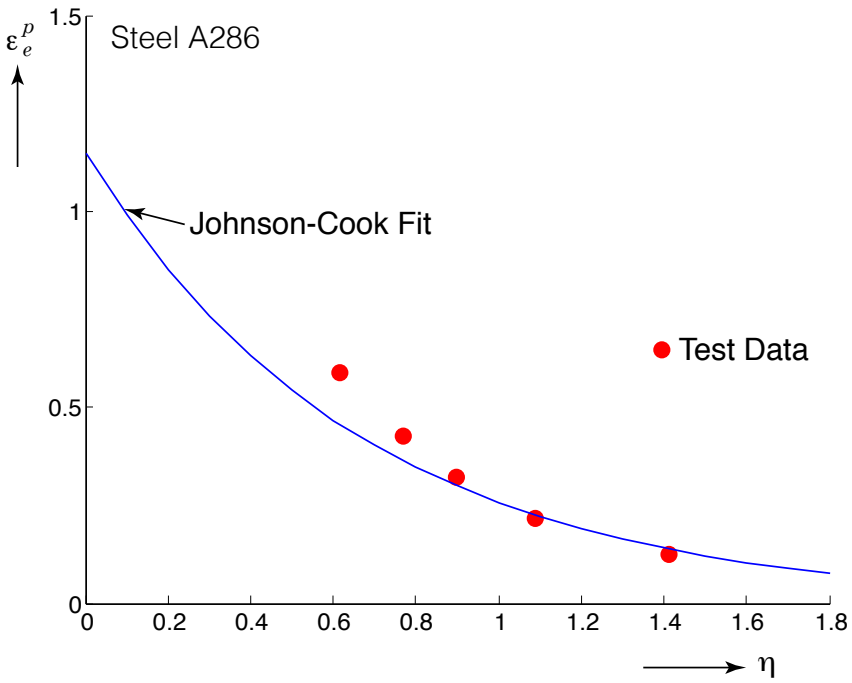

Figure 14. Calibration curve based on notch and smooth specimen tension test data. $d_1 = 0$, $d_2 = 1.15$ and $d_3 = -1.8$.

It shows nearly equal trends for both points, and that the damage level at point S3 was only in the order of 0.45. Failure had already occurred in the test specimens by this point.

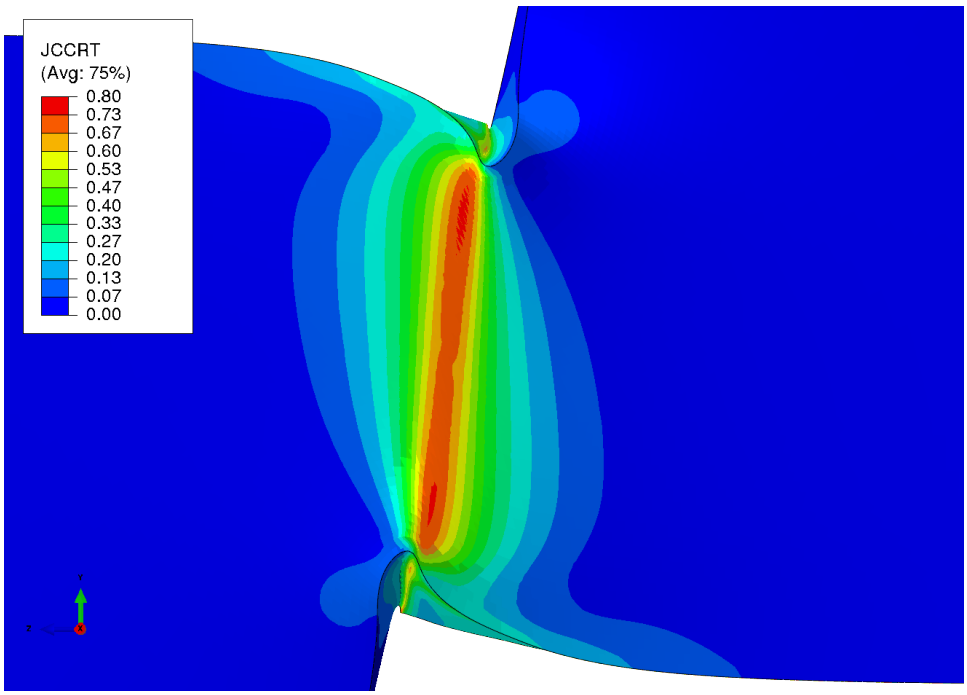

(a)

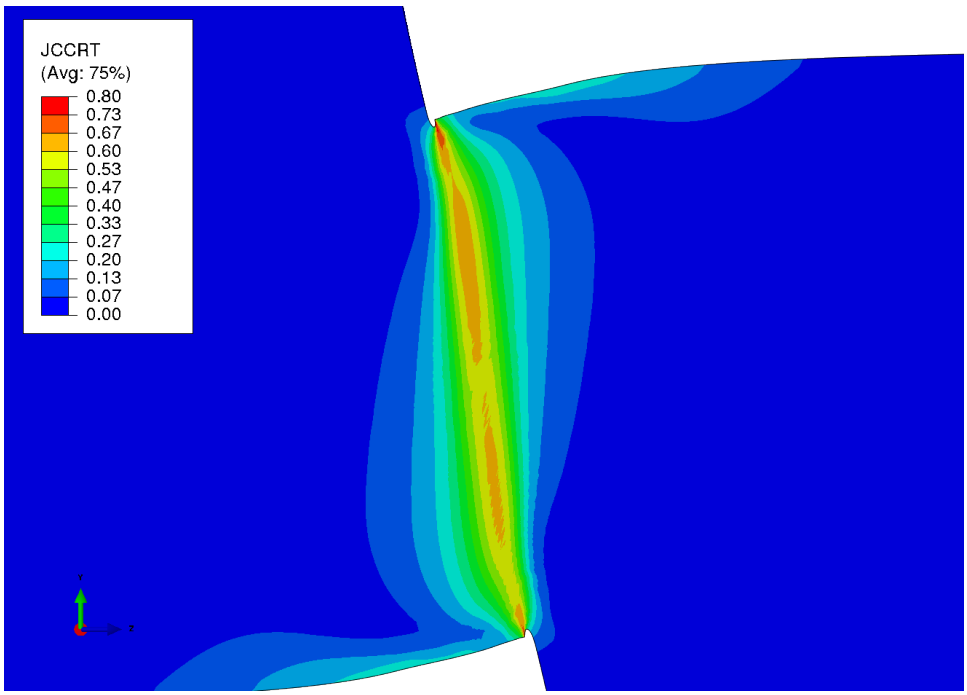

(b)

Figure 15. Damage state in the steel A286 model. (a) At the surface plane and (b) at the center plane.

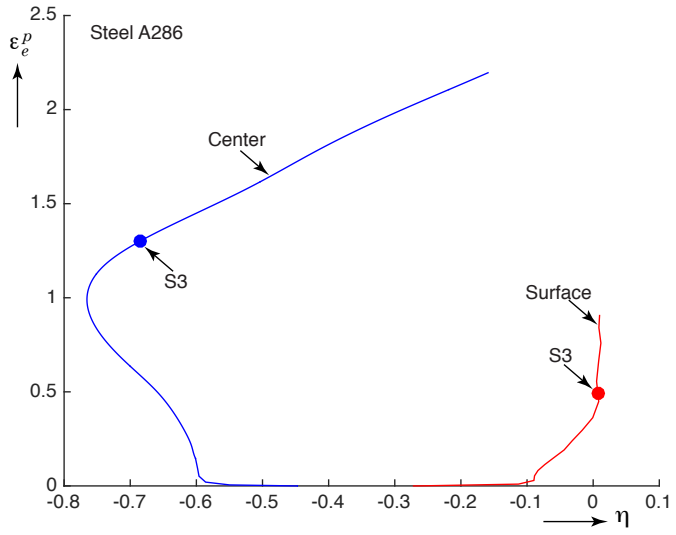

(a)

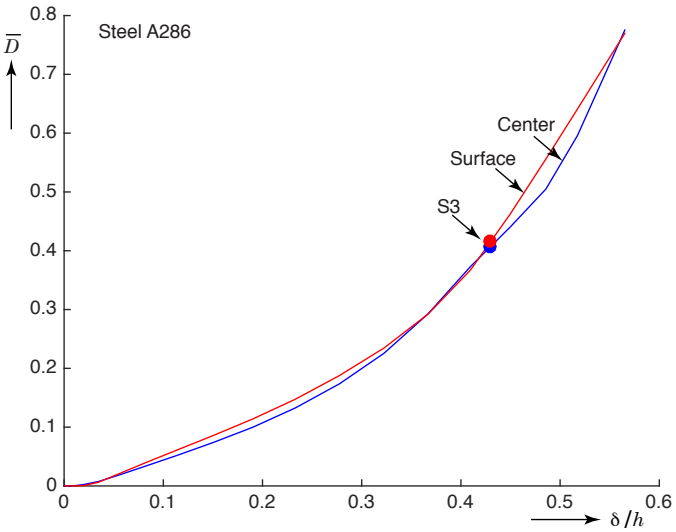

(b)

Figure 16. Damage results for the steel A286 model at the critical locations in the surface and the center planes. (a) Plot of equivalent plastic strain vs. triaxiality and (b) plot of damage vs. displacement.

Imperfection model for Steel A286

Since the evidence presented so far regarding the limit load in the response of the steel A286 specimens points to the development of fracture in the specimen as the source, and since the Johnson-Cook model does not simulate the beginning of failure in the model, an alternative approach was used to induce damage in the model with the intention to check whether a limit load would result in the simulations. The essence of the model is to introduce material imperfections. The finite elements in the model are separated into two groups or phases. The 'first-phase' contains the calibrated models for deformation and failure of steel A286 considered thus far. Only a few percent of the elements, p, are randomly assigned to the 'second-phase,' which still uses the calibrated model for deformation, but its failure is determined simply by specifying a relatively small critical value of equivalent plastic strain at failure, which will be called ε_p. The second phase is the material imperfection. Figure 17 shows one such imperfect model. The elements shown in gray belong to the first phase, while those in blue belong to the second phase. In the example shown, 5% of the elements belong to the second phase. Other than this division of the elements, the simulation is carried out just as before.

Figure 18(a) shows the results obtained when $\varepsilon_p = 0.5$ and p was varied as shown. Note that the model now predicts limit loads for all three cases considered, followed by significant decreases in load. The higher p, the lower the displacement when the maximum load occurs. Similary, holding $p = 1\%$ and changing ε_p in Fig. 18(b) produced load maxima in all cases shown. Interestignly, the trend was non-monotonic. In the last cases presented, Fig. 18(c), the parameters of the second phase were kept constant, but the ductility of the first phase was changed by varying d_2. The higher d_2 the more ductile the first phase is in shear. Increasing d_2 did not significantly influence the displacement at which the load maximum occurred, but decreased the rate at which the load dropped.

To illustrate how the imperfect model behaves, consider the case with $p = 5\%$, $\varepsilon_p = 0.5$ and $d_2 = 2$ shown in Fig. 18(c). This case was chosen because the load-deflection response resembles that of the test data the best of all the cases attempted. The load-deflection response was re-plotted in Fig. 19 with a few points marked along the curve. These points correspond to configurations presented in Fig. 20. Up to point 1, the load-deflection response was smooth. The simulation was conducted with explicit dynamics but the response was smooth because the model was well-behaved, the load was applied smoothly and the effects of inertia were not important. Figures 20(a) and (b) show the state of the specimen in the region of interest, with the damage in the second phase and in the first phase respectively. The plane in the foreground is the center plane. The variable DUCTCRT represents the damage by the critical equivalent plastic strain criterion that only affects the second phase while the variable JCCRT represents the Johnson-Cook damage in the first phase. Material failure takes place when the damage variables reach a value of one. At that time, the elements that have 'failed' are removed from the model. Clearly, the largest values of JCCRT were very small at this point in the loading, but DUCTCRT had almost reached a value of one in the fillet, especially near the center plane where the equivalent plastic strain was highest.

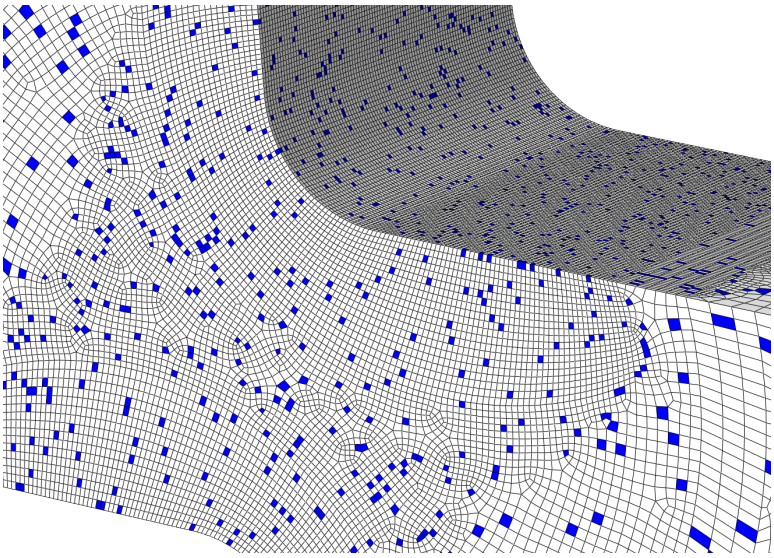

Figure 17. Imprefect finite element model where 5 percent of the elements have been assigned to a second phase to fail when their equivalent plastic strain reaches a critical value.

A little past point 1 in Fig. 17 the load-defection curve became jagged. This is an indication that failure was taking place. The jaggedness in the curve was due to elements being deleted that disturbed the model in ways that excited its dynamic response, and that was reflected in the calculated load. Figure 20(c) shows JCCRT at point 2 in the curve. Interestingly, having deleted a few second-phase elements caused the value of JCCRT in the first phase to jump to 1 in the fillet, thus causing some first phase elements to also fail and be deleted. Note that the damage in the model was biased towards the center plane.

The maximum load occured at about point 3, and the model is shown, now looking straight at the center plane, in Fig. 20(d). Note that the areas where elements had been lost were restricted to small regions at the top and bottom of the shear dominated zone. The model did not include self-contact, so elements were allowed to interpenetrate as is apparent in the figure. This is not thought to be consequential because the objective of the model was just to illustrate the effects of the initiation and some propagation of failure. Still one can see that, as in the tests, having relatively small regions with damage was sufficient to induce the limit load in the response. Points 4 and 5 are in the part of the curve where the load decreased and the respective states of the model at the center plane are shown in Figs. 20(e) and (f) respectively. Although the propagation of failure in the model did not reflect all test observations (for example, the surface plane remained relatively free of damage, whereas in the test the surface plane had the most crack growth), it shows the development of a very localized zone of damage, where more second phase elements were removed, as well as the development of the indentations at the top and bottom surfaces of the high shear zone (they were more symmetric in the tests).

Two issues with some consequence when looking at the results of the model are: (1) some of

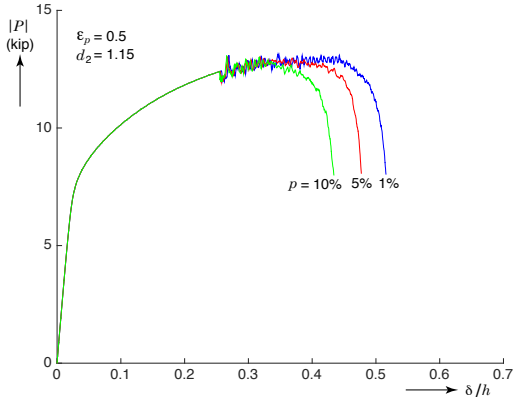

(a)

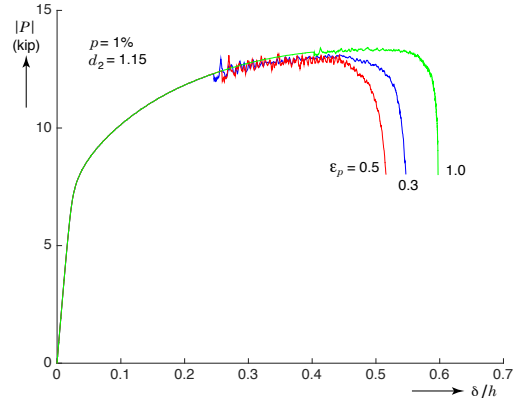

(b)

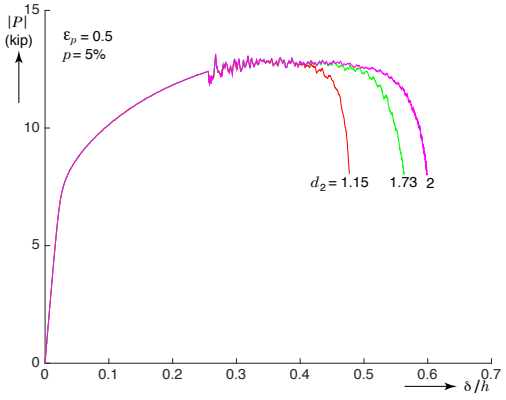

(c)

Figure 18. Results of the imperfect model. (a) Vary the percentage of elements assigned to the second phase, (b) vary the equivalent plastic strain to failure of the second phase and (c) vary the toughness of the first phase.

the element shapes got a bit ugly in the regions where failure was occurring, thus bringing up the question of whether the numerics was the main factor that induced element deletions in the first phase and (2) the response of the model was sensitive to the element size used. The element size was kept at 0.002 inches in all cases, but separate analysis in plane strain surrogates demonstrated this fact. Furthermore, it is very likely that other numerical parameters such as hourglass stiffness, viscosity and damping in the model could affect the results as well. Still, the model results do have some value by demonstrating that introducing a source for damage has the effect of introducing a limit load in the response of the specimens, as was observed in the tests. Also, the model showed that relatively little damage is required to induce the maximum load.

Many open questions remain. A few of them are, for example, what failure criterion should we use to detect first failure for steel A286? Would including dependence on the Lode angle be necessary or at least help? What effect do the inclusions and the surface defects have on the initiation of failure? Since the response of the specimen is influenced by the propagation of cracks it is important to account for it to capture the response accurately, so, how can we model that? Clearly much work remains to try to answer these questions. Only further work that combines test and analysis can be expected to yield some answers. One thing that has been reinforced by the results obtained here is that different failure models are needed for different materials. In addition, the loading history can also be critical in the choice of the failure models. These are examples of well-know deficiencies of phenomenological models such as the ones used here. Yet, they remain as the main tools that can be used for the engineering analysis of ductile failure.

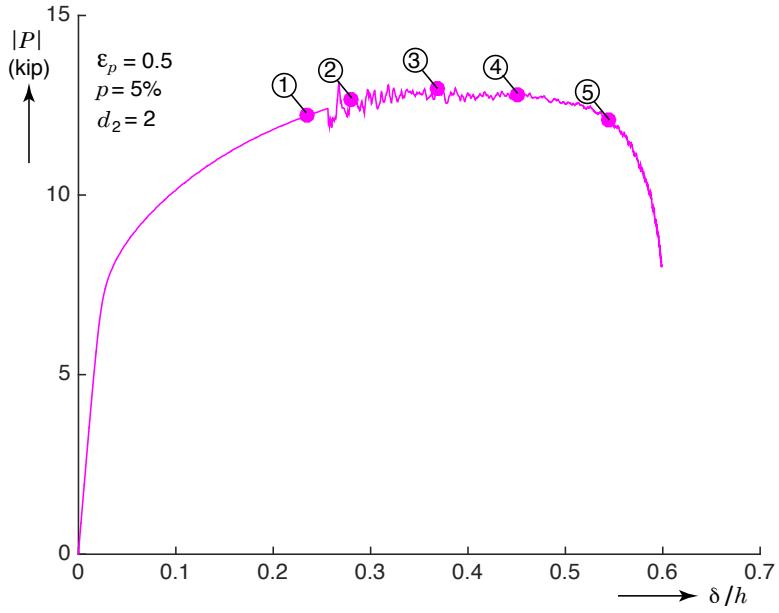

Figure 19. Load-deflection response calculated for the case with $\varepsilon_p = 0.5$, $p = 5\%$ and $d_2 = 2$.

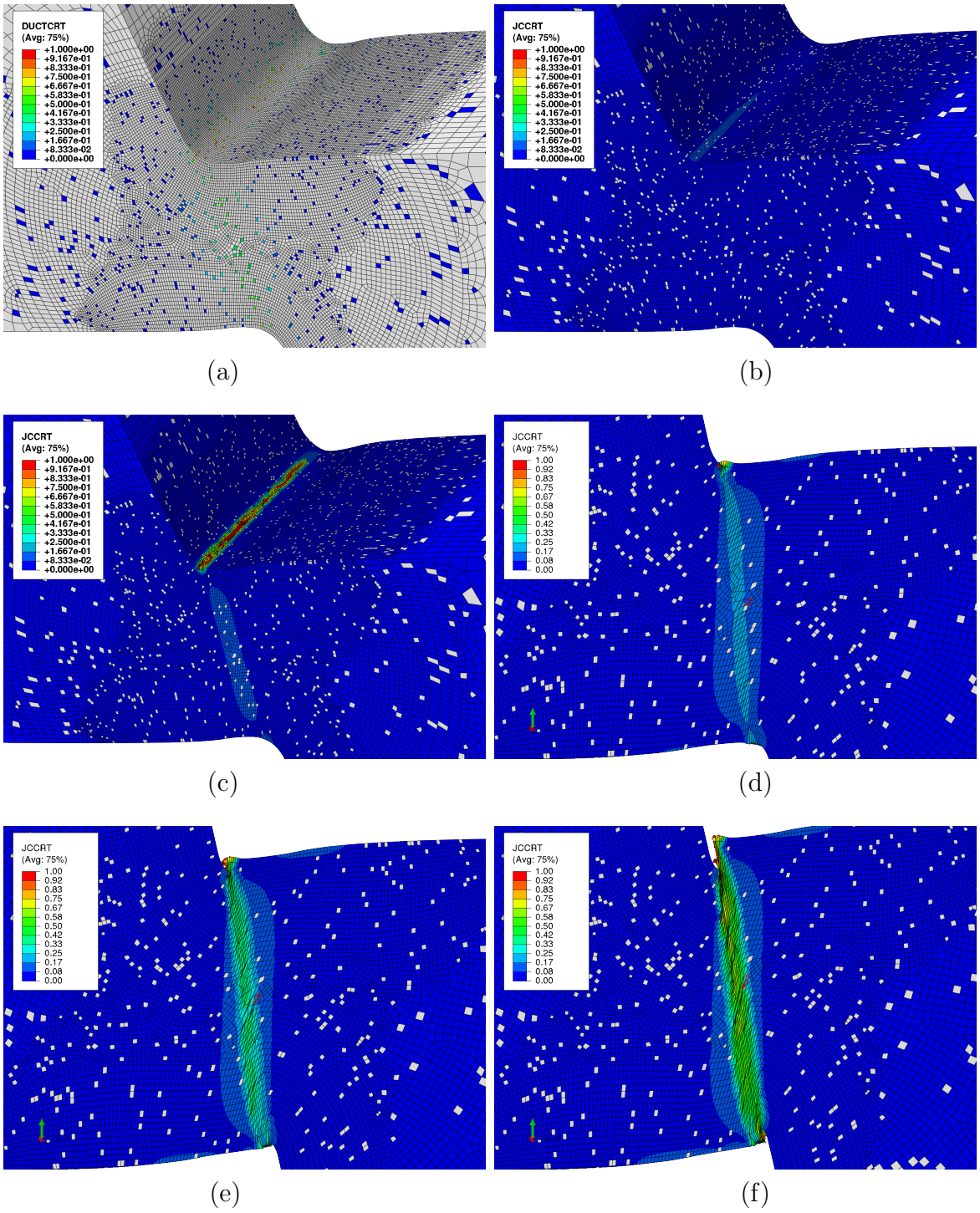

Figure 20. (a) Damage due to equivalent plastic strain criterion at point 1 in Fig.19, (b) Damage due to Johnson-Cook failure at 1, (c) damage due to Johnson-Cook failure at 2, (d) damage due to Johnson-Cook failure at mid-plane at 3, (e) damage due to Johnson-Cook failure at center plane at 4, (f) damage due to Johnson-Cook failure at center plane at 5.

Acknowledgments

Sandia National Laboratories is a multi-mission laboratory managed and operated by Sandia Corporation, a wholly owned subsidiary of Lockheed Martin Corporation, for the U.S. Department of Energy's National Nuclear Security Administration under contract DE-AC04-94AL85000.

References

[1] Corona, E., Deibler, L.A., Reedlunn, B., Ingraham, M.D. and Williams, S., An experimental study of shear-dominated failure in the 2013 Sandia Fracture Challenge specimen, Sandia Technical Report SAND2015-2850, 2015.

[2] Johnson, G.R. and Cook, W.H., Fracture characterization of three metals subjected to various strains, strain rates, temperatures and pressures, *Engineering Fracture Mechanics*, V. 21, pp. 31–48, 1985.

[3] Corona, E. and Orient, G.E., An evaluation of the Johnson-Cook Model to Simulate Puncture of 7075 Aluminum Plates, Sandia Technical Report SAND2014-1550, 2014.

Internal Distribution:

1	0840	E. Fang	1554
1	0840	B. Reedlunn	1554
1	0886	L. Deibler	1819
1	0886	S. Williams	1831
1	0889	B. Boyce	1851
1	9042	A. Brown	8259
1	9042	J. Ostien	8343